Direct measurement of surface charge distribution in phase separating supported lipid bilayers

Thomas Fuhs†[1,2], Lasse Hyldgaard Klausen†[2,3], Steffan Møller Sønderskov[2], Xiaojun Han[1*], Mingdong Dong[2,3*]

1) State Key Laboratory of Urban Water Resource and Environment, School of Chemistry and Chemical Engineering, Harbin Institute of Technology, 92 West Da-Zhi Street, Harbin, 150001, China

2) Interdisciplinary Nanoscience Center (iNANO), Aarhus University, Gustav Wieds Vej 14, Aarhus C, DK-8000, Denmark

3) Department of Chemistry, Stanford University, Stanford, CA 94305, USA

†) These authors contributed equally to this work.

*) To whom correspondence should be addressed, MD: dong@inano.au.dk, XH: hanxiaojun@hit.edu.cn

Abstract

The local surface charge density of the cell membrane influences regulation and localization of membrane proteins. The local surface charge density could, until recently, not be measured directly under physiological conditions, and it was largely a hypothetical yet very important parameter. Here we use unsaturated lipids of distinct charge (DOTAP, DOPC, DOPG) and a neutral fully saturated lipid (DPPC) to create model membranes with phase separating domains of defined charge. We then apply quantitative surface charge microscopy (QSCM) to investigate the local surface charge density; this is a technique based on the scanning ion conductance microscope (SICM) capable of measuring surface charge density with nanoscale lateral resolution. We are able to clearly distinguish lipid domains from charge and topography in all three model membranes. The measured surface charge densities furthermore reveal that disordered domains formed by charged lipids are in fact not pure, but also incorporate uncharged saturated lipids. We estimate that at least 30% of disordered domains in DOPG:DPPC and DOTAP:DPPC will be DPPC. These ratios could present a limit for the formation of charged domains in lipid membranes.

Keywords

Scanning Ion Conductance Microscopy (SICM),
Quantitative Surface Charge Microscopy (QSCM),
Surface charge density,
phase separating lipid bilayer membranes,
charged lipids,
DPPC DOTAP DOPG DOPC

Introduction

Membrane proteins are a vital class of proteins providing a range of functionalities in and across the cell membrane, such as signaling and transport. Transmembrane proteins possess a hydrophobic center and hydrophilic edge parts, which enable them to span the hydrophobic core of the lipid bilayer cell membrane structure.[1] Hydrophilic and hydrophobic interactions ensure the position of the protein in the membrane, but recent advances have shown that also interactions with charged lipids on the bilayer surface are important for protein binding and function.[2] Biological membranes contain a noticeable fraction of charged lipids[3], which can be distributed in smaller regions whose regulation and localization are essential for the biological functions of the cell.[4, 5] *In vitro* experiments have furthermore shown that charged membranes promote amyloid polymerization and thereby membrane disruption.[6-8] The role of localized membrane charge has however mainly been neglected, as it has proven elusive to current measurements methods.[9]

The cell membrane consists of lipids and proteins, and the structure is often heterogeneous with different combinations of lipids and proteins in specific domains.[10] A lipid membrane normally displays a certain degree of fluidity, and mixtures of different lipids tend to organize into separate domains driven by entropic affinity of lipids with similar tail groups.[11] Repulsion between lipids of same charge opposes the formation of charged domains, although these can occur depending on which of the two effects dominate within a given mixture of lipids. The mixing and demixing of lipids is an area of ongoing research interest, with special interest on systems containing lipids that differ both in their tail group structure and head group charge.[12 13] Mixing of lipids with different tail groups is mainly controlled by heating, where the lipid bilayer can change from a dense packing (gel phase) to a more fluid packing (liquid phase). Solution ions of different valence and concentration affect the interaction between charged lipid, and even low salt concentrations can enhance or reduce phase separation in lipid bilayers.[14] Demixing in lipid bilayers is normally investigated using fluorescent markers. These can only be applied to micrometer sized domains, and as these markers are usually big, they might interfere with the lipid ordering. Furthermore, they give an indication of the ordering of the phase, rather than information about the lipid composition.

The electrostatic charge of a lipid bilayer can be calculated or measured using a variety of methods. In the simplest approach the number density of charges in a membrane is calculated from the ratio of lipids in the membrane, the probability of specific groups in each lipid being charged based on pH and the respective area per molecule of each lipid. This value however has little practical relevance as soon as ions are present in the solution covering the membrane. The charges of the membrane will attract counter ions; these will screen the electric potential or even bind to the membrane in varying degrees. Experimentally, the most common way of describing the surface charge is by using the electrokinetic zeta-potential. This is the potential at the plane of shear, where solution ions are free to diffuse laterally.[15] Zeta potential is routinely measured as a bulk average on samples such as lipid nanoparticles for drug or DNA delivery[16], bacteria and even virus-like particles.[17-19] Samples with heterogeneous surface charge distribution, such as mammalian cells, have however been limited by poor experimental accessibility. We recently developed a method, Quantitative Surface Charge Microscopy (QSCM), to measure the surface charge density of lipid membranes.[9] QSCM is based on scanning ion conductance microscopy (SICM), which uses the ionic current passing through the small (10s of nm) tip of a

glass pipette (Figure 1d). This ionic current is affected by tip-sample distance, surface charge density and applied bias potential, and (QSCM) utilizes these influences to measure the surface charge density (Figure 1e) as a difference in apparent topography between two scans at different bias potentials.

Zwitterionic phospholipids, such as phosphatidylcholine and phosphatidylethanolamine, are common constituents of cell membranes.[20] The net charge of zwitterionic lipids is zero at most relevant pH values, bilayers formed from zwitterionic lipids are however known to possess a small but significant charge.[21] The charge stems from the orientation of the lipid head groups, where the positive and the negative charges are located at different planes within the bilayer.[22, 23] As a consequence, the charges will not cancel out completely. The resulting surface potential depends on the distance between the charge planes, and the sign is given by the outermost charge. Analytical approaches[24] as well as MD simulations[25] have shown that external parameters like pH, salt concentration, ion type and temperature can influence the orientation of the head groups, while experiments have shown the influence of these parameters on the zeta potential.[24, 26]

In this work we characterize the surface charge density (SCD) of mixed lipid bilayers comprised of DPPC and DOPG, DOPC or DOTAP (Figure 1a-c). This is the first characterization of surface charges on phase separating lipids under physiological conditions. This work is also another step towards the goal of creating a spatially resolved SCD-map of the cell surface, which in itself is an interesting topic that could provide insightful information on protein regulation, drug and gene delivery or cell-foreign body interactions. We demonstrate that QSCM is capable of distinguishing domains of charged and uncharged lipids with spatial resolution on the nanoscale. Beyond that, we show that the precision of the measured charge is good enough to deduce the mixing of DPPC into disordered DOPG or DOTAP phase domains. This, to our knowledge, has not been feasible with any other experimental technique.

Methods

Materials

DOTAP (1,2-dioleoyl-3-trimethylammonium-propane), DOPC (1,2-dioleoyl-sn-glycero-3-phosphocholine), DOPG (1,2-dioleoyl-sn-glycero-3-phospho-(1'-rac-glycerol)) and DPPC (1,2- dipalmitoyl-sn-glycero-3-phosphocholine) were purchased from Avanti Polar Lipids, USA. All other chemicals and reagents were acquired commercially at analytical grade.

Preparation of phase separated supported lipid bilayers (SLBs)

Lipids were dissolved in chloroform prior to mixing. Saturated and unsaturated lipids were mixed in a 1:1 (w:w) ratio. Lipids mixtures were dried under a nitrogen stream to evaporate the chloroform. The lipids were then resuspended in DI-water (DPPC:DOTAP) or incubation buffer (DPPC:DOPG, DPPC:DOPC) to a final concentration of 0.5 mg/ml. The incubation buffer was 150mM NaCl, 5mM $CaCl_2$, 10mM HEPES, pH7.3. Lipid mixtures were vortexed and extruded at least 11 times through a 100 nm track etched membrane (Nucleopore™, GE Healthcare, USA) at 60°C. 50 µl vesicle suspension and 300 µl buffer were incubated on freshly cleaved mica for 3 h at 60°C, before slowly cooling the samples to room temperature at a rate of 10°C/h. Incubation was

performed in a sealed environment to prevent evaporation. The cold samples were thoroughly washed with imaging buffer. Throughout the experiments care was taken to prevent drying out of the sample, to exclude this as a source of artifacts.

AFM and QSCM imaging

Mica slices were glued temporarily to stainless steel discs with vacuum grease for incubation and AFM imaging. AFM and QSCM imaging was done in buffer consisting of 150 mM NaCl and 10 mM HEPES adjusted to pH 7.3 with NaOH solution. AFM images were recorded on a Multimode 8 (Bruker) operated in peakforce-QNM mode using Scanasyst-Fluid Probes (Bruker AFM Probes) and tapping forces typically in the range of 300-600 pN and tip radii between 10 and 20 nm. After AFM imaging the mica slices were removed from the stainless steel discs and instantly placed in a petri dish filled with imaging buffer for QSCM imaging, which followed immediately. With this the same sample could be used for AFM and QSCM imaging, yet the exact location of the AFM image was not recoverable for QSCM imaging, due to the necessary change of instruments.

QSCM images were recorded on a XE-Bio (Park) operated in DC-SICM mode. The setpoint was 99% of the free currents and the scan rate 0.3 Hz. For each QSCM image a set of two topographies with bias potentials of +/-100mV were recorded. The free currents ranged from 300 pA to 1200 pA. Comparison of these free currents to FEM-simulations was used to calculate pipette diameters of 30 - 75 nm, see Supplementary Note 2 and Supplementary Table 2. Pipettes were pulled from borosilicate capillaries (BF100-50-10, Sutter) with a P2000 pipette puller (Sutter). The SCD vs charge induced height difference (CIHD) curves were simulated for the pipettes used in this work, and can be found in the Supplementary Figure 4. Topographies were flattened using standard SPM-flattening routines in SPIP (Image Metrology, Denmark). The two flattened topographies were subtracted ('+100mV' – '-100mV' = 'CIHD') and the result filtered with Gaussian filter to remove high frequency noise. Histograms of the height difference image were used to determine the relative charge differences in a scan. To calculate the SCD from the charge induced height difference (CIHD) image a conversion factor was calculated for each pipette used[9]; the used factors ranged from of 5.74 to 6.87 (mC/m²)/nm. The SCD is determined using the distance between two peaks in the histogram of the CIHD image, therefore the width of the broader of the two Gaussian distributions is used as error for the obtained SCDs.

Absolute SCDs were obtained by fitting the triangle spanned by the change in tip-sample distance and its change SCD in one potential curve. The change in tip-sample distance was obtained from comparison with AFM topographies. The data analysis is explained in detail in the supplementary information (Supplementary Figure S1).

Results and discussion

The formation of large domains in lipid bilayers is induced by phase separation between liquid ordered and solid gel phase lipids[27]. A mixture of lipids above and below their respective transition temperatures will lead to the formation of distinct liquid and gel phases, the size of which are determined by the preparation protocol. AFM images of the lipid mixtures formulated in this study show the formation of 4 - 8 nm high bilayers on the mica substrate and separation into large domains of approx. 1-2 nm height difference (Figures 2 a+e, 3 a+e, 4

a+e). These measurements confirmed that the supported lipid bilayers (SLBs) exhibited phase separated domains with domain sizes in the micrometer range. The lateral resolution of SICM, which is in the range of 10s of nanometers with the pipettes used in these experiments, should therefore be sufficient to resolve the domains. The samples were then transferred directly from AFM to SICM to investigate the surface charge of the phase-separated SLBs.

The gel transition temperatures of DOPG and DPPC are -18 and 41°C respectively[28]. Figure 2 b+c show the SICM topographies of the formed DOPG-DPPC-SLBs. The visible domains show three distinct heights; the bare mica support, labeled '1' in the figures, and two kinds of lipid domains labelled '2' and '3'. The height of the domains '2' is 10.1 nm, when imaged with a positive SICM potential, and 4.4 nm with a negative SICM potential. The domains '3' show a height of 12.9 nm and 13.2 nm respectively. The apparent SICM topography is a convolution of the physical topography and a contribution from the charge; hence the SICM topographies alone are not sufficient to correlate the domains to the lipid type. Calculating the relative surface charge density (SCD) can clarify this. In the charge induced height difference (CIHD) image (figure 2d) domains '3' become indistinguishable from the mica background. This region thus carries approximately the same negative charge density as the mica. DOPG is negatively charged, while DPPC is zwitterionic, regions '3' are therefore expected to contain mainly DOPG. Domains '2' have a SCD 34.5 mC/m^2 more positive (using a conversion factor of 6.87 (mC/m^2)/nm)) than the bare mica; these regions must therefore be formed mainly by DPPC. Having distinguished DOPG and DPPC predominant regions, the DOPG region in the SICM images are further recognized as stacked bilayers, where the height of 13.2 nm (relative to mica) matches very well with three times the height of a single DOPG-bilayer a measured by AFM (4 nm). The stacked bilayers may result from the use of calcium, a divalent cation, facilitating the buildup[29, 30] as the ions are trapped between the bilayers, thus stabilizing the structure so that rinsing did not remove the additional bilayers. The absolute SCDs are extracted from the theoretical tip-sample distance vs. SCD curve using the apparent height of the DPPC domain with respect to the mica in the negative bias potential SICM scan and the physical height of DPPC domains measured by AFM as described in Supplementary Figure 1. This approach may seem overly complicated but mica is not a reliable reference point, as its surface charge density and zeta potential are highly environment dependent. [31-33] The domains are assigned values of σ_{DPPC} = +13.1 (±8.5) mC/m^2 and σ_{mica} = σ_{DOPG} = -21.4 (±8.5) mC/m^2 (Figure 2h). The PC head group is zwitterionic and at neutral pH carries no net charge, but a small positive SCD is measured for the DPPC domains. Pure samples of DPPC were also prepared, and an obtained SDC of 11.5 mC/m^2 show that the positively charge phase in the DOPG-DPPC mixture is pure DPPC. The charge density of $\sigma_{DOPG,mix}$ = -21.4 mC/m^2 measured for the DOPG domains in the mixed samples is less negative than patches of pure DOPG on mica, $\sigma_{DOPG,pure}$ = -34.9 (±5.8) mC/m^2.This lower charge density implies that DPPC-lipids are mixing into the disordered DOPG phase, diluting the density of charged lipids. The charged head groups of DOPG can lead to a rearrangement of the DPPC head groups, as compared to the pure DPPC phase, changing the partial charge presented by the DPPC. Treating the DPPC lipids as uncharged and using an area per lipid of $A_{DPPC,\ disordered}$ =72 Å^2 and A_{DOPG} = 69.4 Å^2 [34] results in a ratio of 60% DOPG and 40% DPPC in the disordered phase. Assuming a charge equal to the partial charge of DPPC in pure bilayers results in a ratio of 70% DOPG and 30% DPPC (Figure 5 a). This could present a lower threshold for the content of DPPC in disordered domains in DOPG-DPPC-SLBs.

DOTAP is a well-known lipid in the formulation of model membranes. With a phase transition temperature below 0°C, it is known to lower the overall phase transition temperature when mixed with DPPC.[35] Coexisting gel and fluid phases has also been described in DOTAP-DPPC vesicles with <20mol% DOTAP; higher concentrations could however not be investigated using the standard DSC method.[36] We find that the DOTAP-DPPC mixture behaves very similar to the DOPG-DPPC mixture. AFM scans of the mixture show two distinct domains of 3.9 and 6.3 nm respectively (Figure 3 a+e). In the apparent SICM topographies the DOTAP domain appears several nm higher than the surrounding DPPC at both potentials (Figure 3 b+c), this suggest that it is a stack of more than one bilayer. The relative SCD difference between the two domains is small, with the DOTAP being $\Delta\sigma = 6.0$ mC/m^2 more positive than the DPPC (Figure 3d, g) as calculated using a conversion factor of 5.74 (mC/m^2)/nm) (Supplementary Table 2). Using a thickness of 3.9 nm for a single DOTAP bilayer as measured by AFM and the approach described for the DOPG-DPPC sample, the absolute SCDs are σ_{DPPC} = +10.8 (±2.9) mC/m^2 and σ_{DOTAP} = +16.8 (±2.9) mC/m^2 (Figure 3h). The σ_{DPPC} matches the previously obtained value within margins of error. The estimated number of stacked DOTAP bilayers used is 3, resulting in a stack height of 11.7 nm. The surface charge of the domain in the DOTAP-DPPC sample is again lower than the charge obtained for the pure lipid, σ_{DOTAP} = +30.0 (±5.8) mC/m^2. Similarly as for the DOPG-DPPC SLBs this can be explained by DPPC mixing into the disordered DOTAP domain (A_{DOTAP} = 69.4 Å^2). Treating the DPPC lipids as uncharged would result in a mixing ratio of 70% DOTAP and 30% DPPC, while DPPC lipid retaining its partial charge from pure results in a ratio of 1:1 (Figure 5b). It might be interesting to note, that the surface charge density of DOTAP and the DOTAP-DPPC-mix is higher than reported values of surface charge density for DPTAP (σ_{DPTAP} = 15 mC/m^2)[9], even though the molecular charge is +1e/lipid in both cases, and DOTAP occupies a larger area per lipid than DPTAP.

DOPC and DPPC are two of the most commonly studied model lipid systems, but the phase behavior of mixtures containing the two lipids is complex and can include the existence of both compositional and immiscible regions[27, 37]. Both lipids are zwitterionic, and the similar charge readily leads to the formation of large SLB domains, as seen with AFM (Figure 4a,e). SICM topographies show little difference in surface charge between the domains, with one domain 0.7 nm higher on the positive and 1.3 nm higher on the negative bias potential (Figure 4 b,c,f). The CIHD image shows an average height difference of 0.6 nm (Figure 4 d,g). With a conversion factor of 6.62 (mC/m^2)/nm) for this pipette, this corresponds to a small but measurable difference between σ_{DOPC} and σ_{DPPC} of $\Delta\sigma = 3.7$ mC/m^2. The DOPC areas correspond to the lower regions in the SICM scans, but they carry the more positive SCD. Comparison of the SICM topography at -100mV and the AFM scan gives σ_{DOPC} = +12.3 (±2.3) mC/m^2 and the σ_{DPPC} = +8.6 (±2.0) mC/m^2. This value is still within errors of the σ_{DPPC} measured in the DOPG-DPPC experiment. The positive surface charge for the phosphatidylcholines is surprising at first glance, as this head group is normally reported to possess a slightly negative zeta potential in most works. But phosphatidylcholines have also been shown to attain a wide range of zeta potentials depending on external conditions, most notably pH, temperature and salt concentration.[38-40] While neutral pH and room temperature are conditions commonly found in literature, most zeta potential values are recorded at low salt concentrations, typically less than 10 mM. However, the zeta potential of the zwitterionic lipids shifts towards more positive values with increasing salt concentration (Supplementary Figure 2). For DPPC, and other phosphatidylcholines, a change in sign can be experienced with increasing salt concentration, and for 150 mM

NaCl both negative and positive potentials have been reported.[41-43] That DOPC is slightly more positive than DPPC has also been reported previously, although for different conditions.[44] The PC head group is zwitterionic in nature, and the charged subunits sit at considerable distances from each other. The head group possesses some rotational freedom such that the average position of the amine charge relative to the plane defined by the phosphate groups is variable. If the amine charges are not perfectly in plane with the phosphate charges, the lipids carry a partial charge. Lipid areas[45] of A_{DOPC} = 72.1 Å² and A_{DPPC} = 48.6 Å² combined with the measured SCDs equals partial charges of DOPC = 0.06 *e*/lipid and DPPC = 0.03 *e*/lipid. MD-simulation studies showed that the angle of the PC head group changes with changing area of the lipid, and salt concentration has a pronounced influence on the angle[25]. The salt concentration used in this study mimics physiological conditions, but simulation studies matching the experimental conditions were not available in the existing literature.

The AFM and QSCM imaging performed in the work was done on separate setups, this is a limitation as it prevents imaging the exact same spot. But it is not critical for this work as the properties of SLBs are conserved over very long ranges. But for future applications it might be beneficial to use a system that allows imaging the same location with AFM and QSCM, either by using a system that allows changing between AFM and SICM head without moving the sample,[46] or using hollow AFM probes that are capable of SICM imaging.[47]

Conclusions

This paper presents the first quantitative measurement of surface charge density of regions in biologically relevant model membranes, under physiologically relevant conditions. We demonstrate that QSCM is capable of measuring the absolute effective surface charge density of phase separating lipid mixtures, and that the method can differentiate between domains of different SCD, not only for the obvious examples of a charged and uncharged lipid, but also between domains of lipids with the same head group. Characterization of DOPG:DPPC and DOTAP:DPPC mixtures revealed the existence of pure ordered DPPC domains and mixed unordered DOPG and DOTAP domains containing at least 30% DPPC. To our knowledge, such characterization is not feasible with any other method. In the future, QSCM could provide valuable information on the charge distribution of actual cell membranes and how the charge distribution influences the interaction of the membrane with proteins, viruses or nanoparticles. The ability to distinguish between different domains of lipids with the same head group, and to estimate the mixing ratio in domains, will allow new insights into the domain formation of membranes. As QSCM is not dependent on the use of labels, and the employed bias potentials are low, it has a wide range of potential applications.

Conflicts of interest

There are no conflicts to declare.

Acknowledgement

This work was supported by the National Natural Science Foundation of China (Grant no. 21528501, 21650110452), China Postdoctoral Science Foundation (2016M601432), and the Open Funds of the State Key Laboratory of Electroanalytical Chemistry (SKLEAC201707). LHK acknowledges support from the Carlsberg

Foundation Internationalization Fellowships. We also acknowledge the Danish Research Council, AUFF NOVA-project from Aarhus Universitets Forskningsfond and EU H2020 RISE 2016---MNR4SCell project.

References

1. H. Lodish, A. Berk, S. L. Zipursky, P. Matsudaira, D. Baltimore and J. Darnell, *National Center for Biotechnology Information's Bookshelf*, 2000.
2. P. L. Yeagle, *Biochimica et Biophysica Acta (BBA) - Biomembranes*, 2014, **1838**, 1548-1559.
3. J. D. Nickels, J. C. Smith and X. Cheng, *Chemistry and Physics of Lipids*, 2015, **192**, 87-99.
4. M. Edidin, *Annual Review of Biophysics and Biomolecular Structure*, 2003, **32**, 257-283.
5. B.-C. Suh and B. Hille, *Annual Review of Biophysics*, 2008, **37**, 175-195.
6. J. D. Knight and A. D. Miranker, *Journal of Molecular Biology*, 2004, **341**, 1175-1187.
7. T. L. Williams and L. C. Serpell, *Febs J*, 2011, **278**, 3905-3917.
8. H. Ahyayauch, M. Raab, Jon V. Busto, N. Andraka, J.-Luis R. Arrondo, M. Masserini, I. Tvaroska and Félix M. Goñi, *Biophysical Journal*, 2012, **103**, 453-463.
9. L. H. Klausen, T. Fuhs and M. Dong, *Nat Commun*, 2016, **7**.
10. G. M. Cooper and R. E. Hausman, *The cell*, Sinauer Associates Sunderland, 2000.
11. S. Semrau and T. Schmidt, *Soft Matter*, 2009, **5**, 3174-3186.
12. A. Chung, *Nature Reviews Molecular Cell Biology*, 2009, **10**, 442-443.
13. A. Callan-Jones, B. Sorre and P. Bassereau, *Cold Spring Harbor perspectives in biology*, 2011, **3**, a004648.
14. H. Himeno, N. Shimokawa, S. Komura, D. Andelman, T. Hamada and M. Takagi, *Soft Matter*, 2014, **10**, 7959-7967.
15. A. V. Delgado, F. González-Caballero, R. J. Hunter, L. K. Koopal and J. Lyklema, *J Colloid Interf Sci*, 2007, **309**, 194-224.
16. Y. Wang, S. Gao, Y. Wen-Hui, H. S. Yoon and Y. Yi-Yan, *Nature materials*, 2006, **5**, 791.
17. I. Samandoulgou, I. Fliss and J. Jean, *Food and Environmental Virology*, 2015, **7**, 249-260.
18. W. W. Wilson, M. M. Wade, S. C. Holman and F. R. Champlin, *Journal of Microbiological Methods*, 2001, **43**, 153-164.
19. C. Ayala-Torres, N. Hernández, A. Galeano, L. Novoa-Aponte and C.-Y. Soto, *Ann Microbiol*, 2014, **64**, 1189-1195.
20. G. van Meer and A. I. de Kroon, *J Cell Sci*, 2011, **124**, 5-8.
21. F. Pincet, S. Cribier and E. Perez, *The European Physical Journal B-Condensed Matter and Complex Systems*, 1999, **11**, 127-130.
22. R. H. Pearson and I. Pascher, *Nature*, 1979, **281**, 499-501.
23. E. C. Mbamala, A. Fahr and S. May, *Langmuir*, 2006, **22**, 5129-5136.
24. K. Makino, T. Yamada, M. Kimura, T. Oka, H. Ohshima and T. Kondo, *Biophysical Chemistry*, 1991, **41**, 175-183.
25. A. A. Gurtovenko, *The Journal of Chemical Physics*, 2005, **122**, 244902.
26. R. Zimmermann, D. Küttner, L. Renner, M. Kaufmann, J. Zitzmann, M. Müller and C. Werner, *Biointerphases*, 2009, **4**, 1-6.
27. G. van Meer, D. R. Voelker and G. W. Feigenson, *Nat Rev Mol Cell Biol*, 2008, **9**, 112-124.
28. E. J. Findlay and P. G. Barton, *Biochemistry*, 1978, **17**, 2400-2405.

29. S. Nir, J. Bentz, J. Wilschut and N. Duzgunes, *Progress in Surface Science*, 1983, **13**, 1-124.
30. D. Leckband, C. Helm and J. Israelachvili, *Biochemistry*, 1993, **32**, 1127-1140.
31. D. L. Dolcater, E. G. Lotse, J. K. Syers and M. L. Jackson, *Soil Science Society of America Journal*, 1968, **32**, 795-798.
32. A. Nosrati, J. Addai-Mensah and W. Skinner, *Chem Eng J*, 2009, **152**, 406-414.
33. P. J. Scales, F. Grieser and T. W. Healy, *Langmuir*, 1990, **6**, 582-589.
34. J. Pan, F. A. Heberle, S. Tristram-Nagle, M. Szymanski, M. Koepfinger, J. Katsaras and N. Kučerka, *Biochimica et Biophysica Acta (BBA) - Biomembranes*, 2012, **1818**, 2135-2148.
35. S. Cinelli, G. Onori, S. Zuzzi, F. Bordi, C. Cametti, S. Sennato and M. Diociaiuti, *The Journal of Physical Chemistry B*, 2007, **111**, 10032-10039.
36. R. B. Campbell, S. V. Balasubramanian and R. M. Straubinger, *Biochimica et Biophysica Acta (BBA)-Biomembranes*, 2001, **1512**, 27-39.
37. S. J. Attwood, Y. Choi and Z. Leonenko, *Int J Mol Sci*, 2013, **14**, 3514-3539.
38. M. A. Morini, M. B. Sierra, V. I. Pedroni, L. M. Alarcon, G. A. Appignanesi and E. A. Disalvo, *Colloids and Surfaces B: Biointerfaces*, 2015, **131**, 54-58.
39. M. d. C. Luzardo, G. Peltzer and E. A. Disalvo, *Langmuir*, 1998, **14**, 5858-5862.
40. H. Egawa and K. Furusawa, *Langmuir*, 1999, **15**, 1660-1666.
41. K. Makino, T. Yamada, M. Kimura, T. Oka, H. Ohshima and T. Kondo, *Biophysical chemistry*, 1991, **41**, 175-183.
42. S. Yokoyama, A. Inagaki, T. Imura, T. Ohkubo, N. Tsubaki, H. Sakai and M. Abe, *Colloids and Surfaces B: Biointerfaces*, 2005, **44**, 204-210.
43. Y. Park, R. Huang, D. S. Corti and E. I. Franses, *J Colloid Interf Sci*, 2010, **342**, 300-310.
44. E. Chibowski and A. Szcześ, *Adsorption*, 2016, **22**, 755-765.
45. J. F. Nagle and S. Tristram-Nagle, *Biochimica et Biophysica Acta (BBA) - Reviews on Biomembranes*, 2000, **1469**, 159-195.
46. T. Ushiki, M. Nakajima, M. Choi, S.-J. Cho and F. Iwata, *Micron*, 2012, **43**, 1390-1398.
47. D. Ossola, L. Dorwling-Carter, H. Dermutz, P. Behr, J. Vörös and T. Zambelli, *Physical Review Letters*, 2015, **115**, 238103.

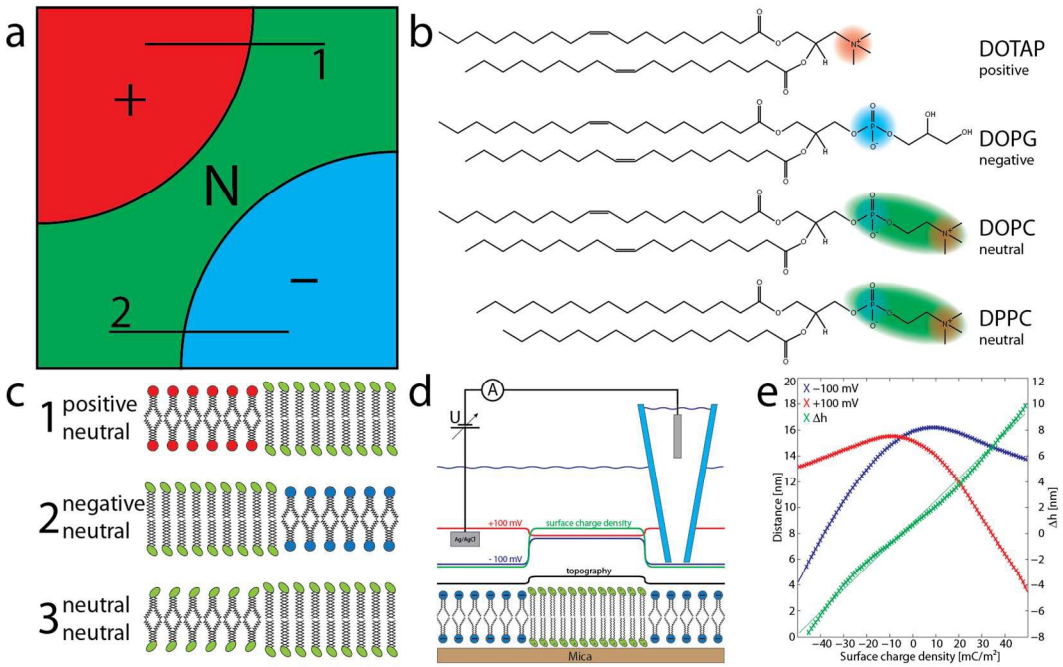

Figure 1: a) A domain of pure lipids can have 3 distinct charge states, positive, neutral or negative. A phase separating mixture of these two can come in the variants 1: positive/neutral, 2: negative/neutral, 3: neutral/neutral

b) The used lipids: DOTAP (positive charge), DOPG (negative charge), DOPC (zwitterionic, neutral charge at neutral pH values). These three will be in a liquid disordered phase at room temperature. DPPC is zwitterionic and will be in the liquid ordered phase at room temperature and is thus expected to phase separate from the others lipids.

c) Schematic of the used SLBs, 1: DOTAP:DPPC, 2: DOPG:DPPC, 3: DOPC:DPPC.

d) Experimental setup of for QSCM. A glass pipette with a nanoscale tip is scanned over the sample. During scanning a bias voltage is applied between an Ag/AgCl-electrode in the pipette and one in the bulk solution. The resulting current is used as feedback parameter for the vertical position, as the current is strongly dependent on the tip-sample distance. A minor influence stems from the surface charge density of the sample and the bias potential. The apparent topography recorded with SICM will differ from the actual topography, when a surface of varying charge is scanned.

e) The tip-sample distance is dependent on the surface charge density as well as the bias potential. The difference between the two tip-sample distances at the two bias potentials gives the charge induced height difference, Δh, which is almost a linear function of the surface charge density. The slope is 5.78 mCm^{-2}/nm.[9]

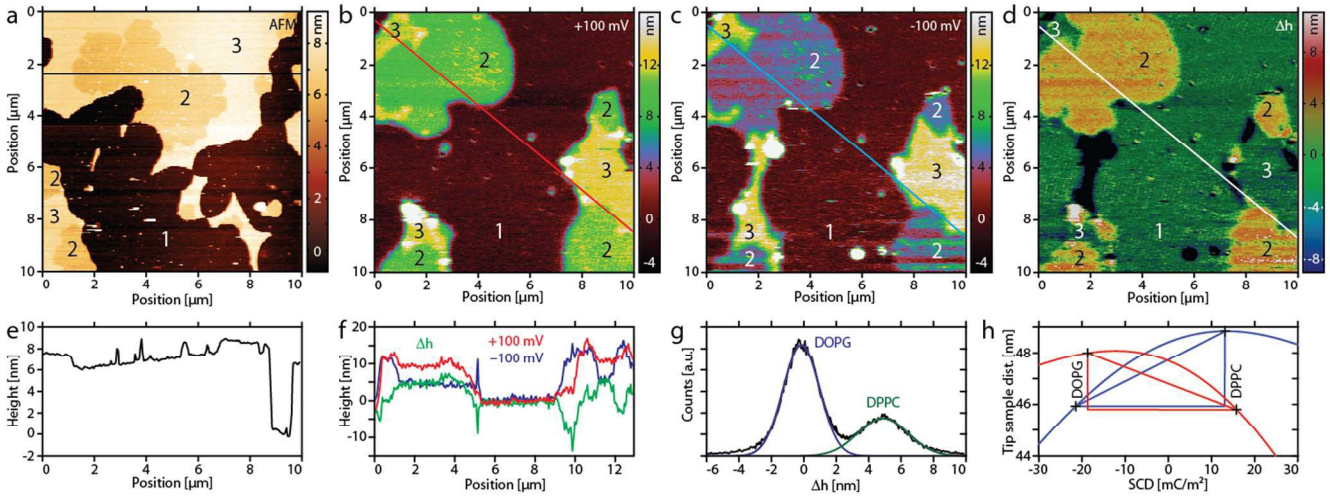

Figure 2) DOPG:DPPC. a) The AFM image of phase separating domains of DOPG (3) and DPPC (2) on mica (1), the DOPG has formed a double bilayer with height 8nm and the DPPC is a single bilayer of height 7 nm. The apparent SICM topographies b), c) show three domains of distinct height 1: mica support, 2: DPPC (10.1 nm and 4.4 nm), 3: DOPG:DPPC-mix (12.9 nm and 13.2 nm). The CIHD-image d) calculated from b) and c) shows the difference in height of the two apparent topographies, this is proportional to the effective SCD. Panel f shows a selected line profile from b), c) and d). The physical height of the domains measured from the AFM image a), e) are used to place the relative SCD difference calculated from the histogram g) on the Tip-sample distance vs. SCD curve h) to obtain the absolute SCD values. The tip radius was 37.1 nm.

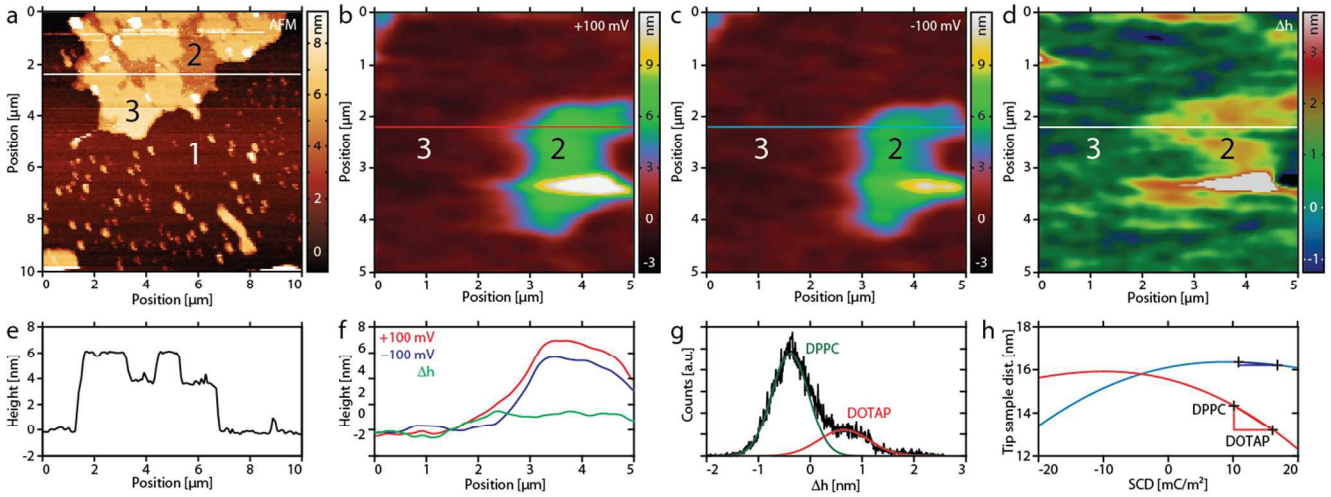

Figure 3) DOTAP:DPPC. The apparent SICM topographies b) and c) show two domains of distinct height, 3: DPPC, 2: DOTAP:DPPC-mix. The DOTAP domain appears several nm higher than DPPC in both topographies; this shows that the domain is a stack of two bilayers. The CIHD-image d) calculated from b) and c) shows the difference in height (1 nm) of the two apparent topographies, this is proportional to the change in effective SCD (6 mC/m^2). Panel f shows a selected line profile from b), c) and d). The physical heights of the domains, (1) mica, 2) DOTAP = 3.9 nm, 3) DPPC = 6.3 nm) measured from the AFM image, a), are used to place the relative SCD difference calculated from the histogram g) on the Tip-sample distance vs. SCD curve h) to obtain the absolute SCD values. The tip radius was 16.8 nm.

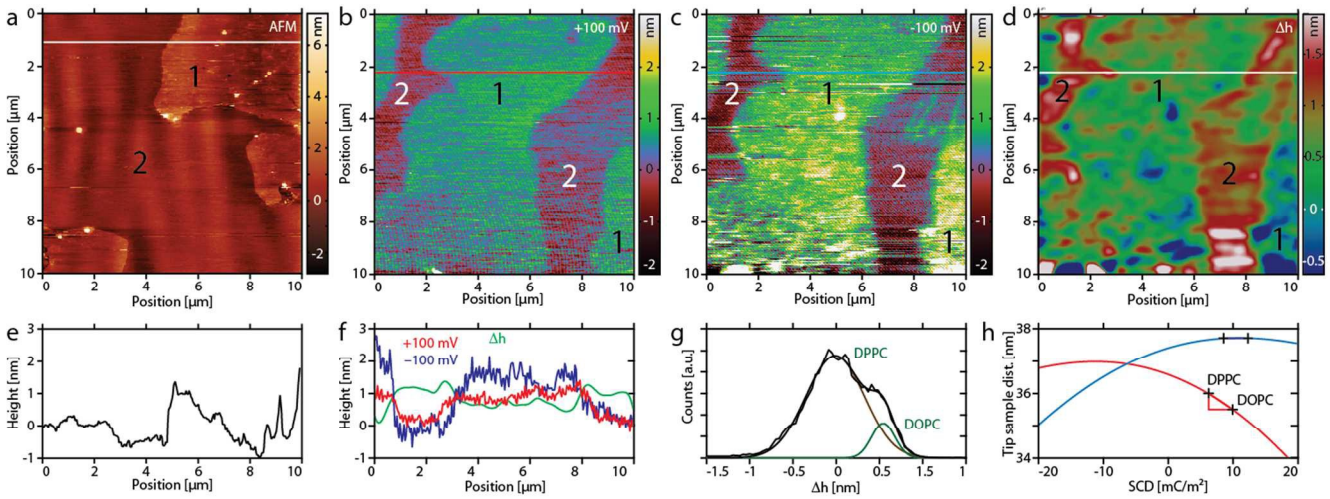

Figure 4) DOPC-DPPC. The apparent SICM topographies b) and c) show two domains of distinct height,1: DPPC, 2: DOPC (0.7 nm and 1.3 nm lower). The CIHD-image d) calculated from b) and c) shows the difference in height of the two apparent topographies, this is proportional to the effective SCD. Panel f) shows a selected line profile from a), b) and d). The physical height of the domains measured from the AFM image a), e) are used to place the relative SCD difference calculated from the histogram g) on the Tip-sample distance vs. SCD curve h) to obtain the absolute SCD values. The tip radius was 29.9 nm.

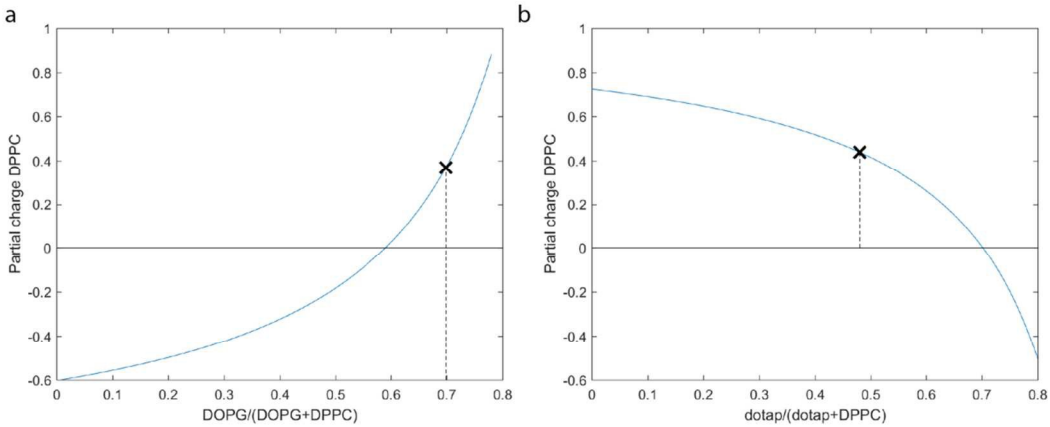

Figure 5)

a) Mixing ratio of the disordered domains in a DOPG-DPPC SLB depending on the partial charge of the DPPC. Assuming the DPPC to be neutral gives a concentration of 60% DOPG, while assuming the same partial charge as the DPPC domains gives a concentration of 70% DOPG.

b) Mixing ratio of the disordered domains in a DOTAP-DPPC SLB depending on the partial charge of the DPPC. Assuming the DPPC to be neutral gives a concentration of 70% DOTAP, while assuming the same partial charge as the DPPC domains gives a concentration of 50% DOTAP.

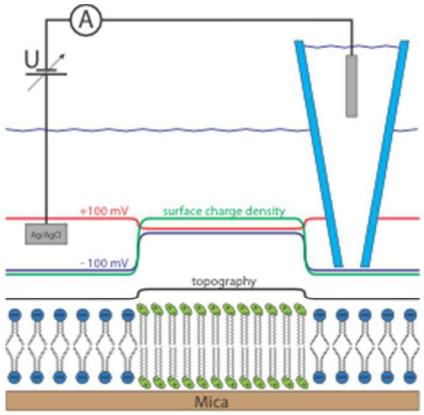
A
U
+100 mV
surface charge density
Ag/AgCl
- 100 mV
topography
Mica

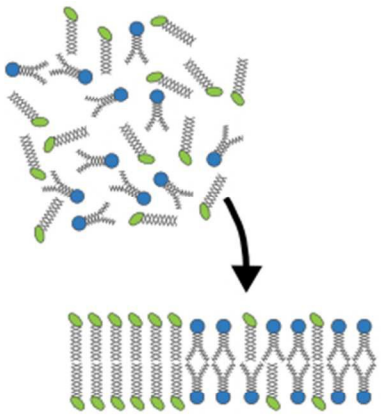

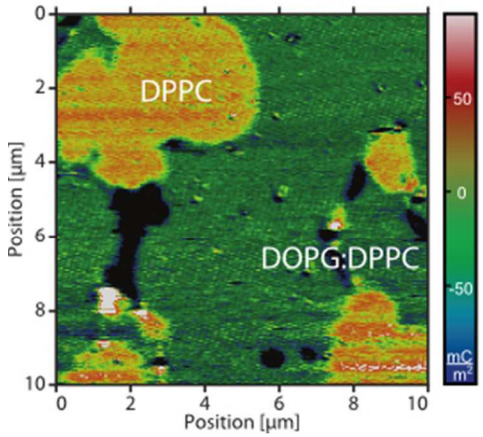
DPPC
DOPG:DPPC
Position [µm]
Position [µm]
50
0
-50
mC
m²

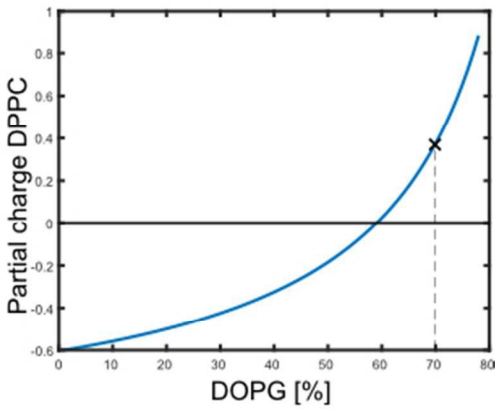
Partial charge DPPC
DOPG [%]